SIMBAD: a field radiometer for satellite ocean-color validation

Pierre-Yves Deschamps, Bertrand Fougnie, Robert Frouin,
Pierre Lecomte, and Christian Verwaerde

A hand-held radiometer, called SIMBAD, has been designed and built specifically for evaluating satellite-derived ocean color. It provides information on the basic ocean-color variables, namely aerosol optical thickness and marine reflectance, in five spectral bands centered at 443, 490, 560, 670, and 870 nm. Aerosol optical thickness is obtained by viewing the Sun disk and measuring the direct atmospheric transmittance. Marine reflectance is obtained by viewing the ocean surface and measuring the upwelling radiance through a vertical polarizer in a geometry that minimizes glitter and reflected sky radiation, i.e., at 45° from nadir (near the Brewster angle) and at 135° in azimuth from the Sun's principal plane. Relative inaccuracy on marine reflectance, established theoretically, is approximately 6% at 443 and 490 nm, 8% at 560 nm, and 23% at 670 nm for case 1 waters containing 0.1 mg m^{-3} of chlorophyll *a*. Measurements by SIMBAD and other instruments during the Second Aerosol Characterization Experiment, the Aerosols-99 Experiment, and the California Cooperative Oceanic Fisheries Investigations cruises agree within uncertainties. The radiometer is compact, light, and easy to operate at sea. The measurement protocol is simple, allowing en route measurements from ships of opportunity (research vessels and merchant ships) traveling the world's oceans.

OCIS codes: 010.1290, 010.4450, 280.0280.

1. Introduction

Since the development of the historical, proof-of-concept Coastal Zone Color Scanner (CZCS),[1] which during 1978–1986 provided the first global ocean-color data set from space, improved satellite ocean-color sensors with global coverage capability have been designed and launched. They include the polarization and directionality of the Earth's reflectance (POLDER) instrument[2] and the ocean color and temperature scanner (OCTS) onboard the Advanced Earth Observing Satellite (ADEOS; November 1996–June 1997); the Sea-viewing Wide Field-of-View Sensor (SeaWiFS)[3] onboard the OrbView-2 satellite (August 1997 to the present); and the Moderate-Resolution Imaging Spectrometer (MODIS)[4] onboard the Terra (December 1999 to the present) and Aqua (May 2002 to the present) satellites. Compared with the CZCS, these new-generation sensors have more adequate spectral bands (e.g., for atmospheric correction) and a higher signal-to-noise ratio. Other wide field-of-view sensors have been launched, namely, the Medium-Resolution Imaging Spectrometer (MERIS)[5] onboard the ENVISAT satellite (March 2002) and POLDER-2 and the Global Imager[6] onboard ADEOS-II (December 2002), and they will contribute to a more complete, global, continuing time series of ocean-color observations.

Processing satellite ocean-color data into chlorophyll *a* concentration, diffuse attenuation coefficient, or other variables characterizing the water body involves removing unwanted atmospheric effects. At ocean-color wavelengths, i.e., in the blue and green, only a small fraction of the measured signal (typically 10%) contains useful information in the form of photons that have interacted with the water body. Consequently, accurate atmospheric correction of the top-of-atmosphere signal is necessary to attain acceptable accuracy for the retrieved ocean variables.

The atmospheric contribution is due mainly to scattering by molecules and aerosols. Molecular scatter-

Pierre-Yves Deschamps, Pierre Lecomte, and Christian Verwaerde are with the Laboratoire d'Optique Atmosphérique, Université des Sciences et Technologies de Lille, 59655 Villeneuve d'Ascq, France. Bertrand Fougnie is with the Centre National d'Etudes Spatiales, 18 Avenue Edouard Belin, 31401 Toulouse, France. Robert Frouin (rfrouin@ucsd.edu) is with the Climate Research Division, Scripps Institution of Oceanography, University of California San Diego, 8810 La Jolla Shores Drive, La Jolla, California 92037.

Received 11 July 2003; revised manuscript received 10 March 2004; accepted 5 April 2004.

0003-6935/04/204055-15$15.00/0

ing can be accurately computed from the surface pressure[7,8]; however, aerosol scattering, highly variable in space and time, is difficult to quantify. Atmospheric correction algorithms (e.g., Refs. 9 and 10) generally estimate aerosol scattering from the satellite radiance measured in two spectral bands in the red and near-infrared where the oceanic contribution is very small or negligible (765 and 865 nm) or predictable (670 nm for case 1 waters). From the intensity and spectral dependence of the aerosol scattering at these two wavelengths, aerosol optical thickness and type can be retrieved. This allows computation, therefore correction, of the aerosol scattering at ocean-color wavelengths, yielding water-leaving radiance or, equivalently, marine reflectance. Eventually, bio-optical algorithms are applied to the retrieved water-leaving radiance; see, for example, Austin and Petzold[11] for the diffuse attenuation coefficient at 490 nm and Morel[12] or O'Reilly *et al.*[13] for chlorophyll *a* concentration.

The best way to evaluate the performance of the atmospheric correction is to compare *in situ* measurements, over a wide range of conditions, with values of the variables retrieved by the atmospheric correction scheme. The necessary variables are the marine reflectance, the aerosol optical thickness, and the aerosol model.[14–16] These variables also need to be measured for the vicarious calibration of the sensors while they operate in orbit. In the vicarious calibration procedure, the measurements are used either to compute the satellite signal by using a suitable radiative transfer code and then comparing the modeled signal with the measured signal[17,18] or to evaluate satellite retrievals.[19]

The *in situ* measurements of water-leaving radiance or marine reflectance are usually made with underwater instrumentation by measuring the depth profile of upwelling radiance and downwelling irradiance and by extrapolating the values to the surface and across the air–sea interface. The logistics involved with this approach are not simple. It is necessary to stop the ship and operate a winch, to drift away a free-fall system, or to deploy and maintain buoys.[14,15] Furthermore, dedicated validation campaigns at sea are expensive and may not be cost effective, because cloud cover may drastically limit the number of matchups between satellite estimates and *in situ* measurements.

An alternative to the standard underwater techniques are above-water techniques utilizing radiometers that measure upwelling radiance.[14,20–29] The chief difficulty with the above-water techniques is contamination by Sun glint and skylight reflected in the instrument's field of view, which is not easy to correct. Fougnie *et al.*[25] have shown that the glitter can be avoided and skylight reflection substantially reduced by using a vertical polarizer and viewing the ocean surface in a specific geometry, i.e., 45° from the nadir and 135° from the solar plane. Such water-leaving radiance measurements are easier and faster to make than those with classical underwater instrumentation. A major advantage is that the ship does not need to stop, and the measurements can be obtained without interfering with ship operations. This offers the opportunity to collect data during a variety of research cruises, especially during voyages by merchant ships traveling regular routes in the world's oceans.

In the context of current and future ocean-color missions, and in view of the stated requirements, we have developed a specific, dedicated hand-held radiometer for evaluating satellite-derived ocean color. This radiometer, called SIMBAD, was optimized in terms of design and measurement protocol for easy and regular use onboard volunteer ships. It works like a sunphotometer when aimed at the Sun, and it measures water-leaving radiance when aimed at the ocean surface. From these measurements aerosol optical thickness and marine reflectance can be deduced. Thus the SIMBAD radiometer gives access to the two basic atmospheric and oceanic variables necessary to quantify atmospheric correction performance. In the following text, we present the instrument (including its concept and principle), discuss data processing and accuracy, and compare measurements obtained by SIMBAD and other instruments (sunphotometer and underwater radiometer) during the Second Aerosol Characterization Experiment (ACE-2), the Aerosols-99 Experiment, and the California Cooperative Oceanic Fisheries Investigations (CalCOFI) cruises.

2. SIMBAD Radiometer

A. Concept

Several requirements were considered in the design of the SIMBAD instrument. First, the instrument had to provide concomitant measurements of aerosol optical thickness and water-leaving radiance in typical spectral bands of satellite ocean-color sensors. Second, quality data had to be collectable from any moving platform at sea. Third, cost had to be kept low to allow the manufacture and deployment of a sufficient number of instruments for sampling varied oceanic and atmospheric regimes. In view of these requirements, we opted for a compact, light, and portable filter radiometer operating in two modes, namely Sun-viewing mode for measuring direct solar extinction and sea-viewing mode for measuring water-leaving radiance.

To reduce Sun-glint and skylight-reflection effects in the sea-viewing mode, the instrument measures vertically polarized radiance. A preliminary study theoretically and experimentally identified the optimum viewing angles that minimize the perturbing effects.[25] It was concluded that the radiometric measurements should be made at a nadir angle of 45° (near the Brewster angle) and at a relative azimuth angle of 135° between the solar and the viewing directions. In this configuration the residual reflected skylight in the measured signal is correctable to a few 10^{-4} in reflectance units, and the resulting error on the diffuse marine reflectance in the blue and green wavelengths is less than 1% for most water types.

Table 1. Characteristics of the SIMBAD Radiometer

Parameter	Value
Number of spectral bands	5
Center wavelength (bandwidth)	443 (10), 490 (10), 560 (10), 670 (10), 870 (10) nm
Detector	Silicon photodiodes
Dynamic range	1–500,000 *CN*[a]
Sampling rate	10 Hz
Number of gains	2
Field of view	3°
Weight	~4 kg
Shape, size	Cylindrical, ~40 cm × 15 cm
Batteries	Ni–Cd
Memory	458 Mbytes
Noise-equivalent reflectance[b]	$<2 \times 10^{-5}$

[a]*CN*, number of counts for Sun and sea measurements.
[b]For oceanic applications and for the five spectral bands.

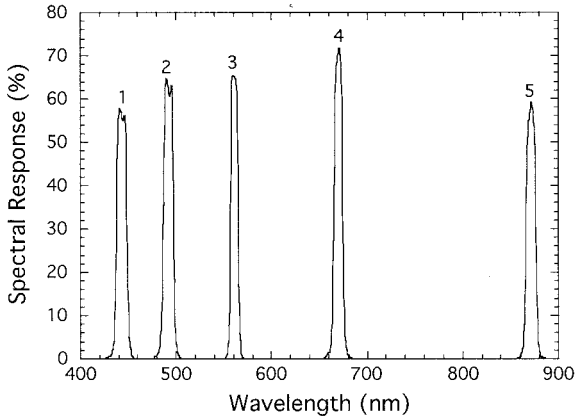

Fig. 1. Spectral response of the SIMBAD instrument. Band 1 is centered on 443 nm, band 2 on 490 nm, band 3 on 560 nm, band 4 on 670 nm, and band 5 on 870 nm.

Krotov and Vasilkov[26] also recommended that angular geometry for polarized measurements be just above the sea surface.

Compared with the viewing geometry for unpolarized measurements suggested by Lee *et al.*[22,23] and used by Toole *et al.*[30] and others (i.e., 30° from nadir and 90° from the solar plane), the viewing geometry for polarized measurements reduces skylight-reflection effects by a factor of 3–4.[25] Another argument in favor of polarized measurements near the Brewster angle is that the residual skylight is much less sensitive to uncertainties in viewing angles, wind speed, and aerosol amount.[25] Measuring sky radiance is not necessary, which simplifies measurement procedures. In addition, aiming the surface at 45° from nadir instead of 30° makes it easier to avoid foam and bubbles generated by ship movement.

Water-leaving radiance depends strongly on the amount of solar radiation reaching the surface (the greater the incident solar irradiance, the greater the water-leaving radiance). It is important, therefore, to normalize water-leaving radiance by downwelling solar irradiance. For example, if the surface measurements are not performed at exactly the time of satellite overpass, the change in solar irradiance between surface and satellite measurements may prevent water-leaving radiance comparisons. The SIMBAD radiometer was not designed to measure downwelling solar irradiance. This variable is computed by use of the aerosol optical thickness measured by the instrument. This computation is accurate under clear-sky conditions (Sun not obscured by clouds), which are the same conditions for satellite ocean-color evaluation—the purpose of the instrument.

B. Description

The main characteristics of the SIMBAD radiometer are summarized in Table 1. Polarized radiance is measured in five spectral bands centered at 443, 490, 560, 670, and 870 nm and approximately 10 nm wide (Fig. 1). These spectral bands are typical of satellite ocean-color sensors and contain the basic information for atmospheric correction and bio-optical modeling. The measurements are made simultaneously in the five spectral bands through five aligned optical subassemblies (Fig. 2). Each subassembly includes a vertical polarizer, interference filter, lens, and silicon detector. The incident signal is acquired at a frequency of 10 Hz and is amplified, digitally converted, and stored internally. The instrument is equipped with a magnetometer and two inclinometers for measuring viewing angles and a Global Positioning System for determining the time and the geographic location. Four lights controlled by the magnetometer and inclinometers help the operator to aim precisely at the surface in the required geometry (45° from nadir and 135° in azimuth with respect to the solar plane). The total field of view is 3°, a good compromise between a small field of view for measuring direct solar extinction (necessary to minimize

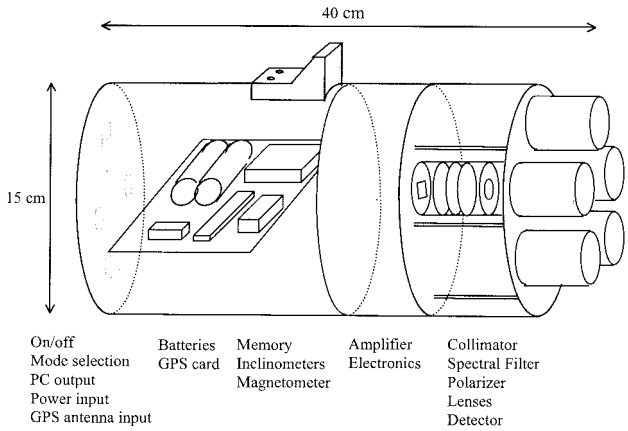

Fig. 2. Diagram of the SIMBAD radiometer. The main parts are five optical subassemblies, including interference filter, lenses, polarizer, and detector (right-hand side); electronic card (middle); memory, GPS, inclinometer, and magnetometer card (left-hand side); and power and GPS antenna input (back face). Only one set of lenses, corresponding to one of the optical subassemblies, is drawn.

atmospheric scattering) and a larger field of view for measuring water-leaving radiance. The polarizers do not affect the measurement of direct solar extinction because direct sunlight is not polarized. The external shape of the instrument is cylindrical, the length is 40 cm, the diameter is 15 cm, and the total weight is 4 kg.

Two electronic gains are used, a low gain in Sun-viewing mode and a high gain in sea-viewing mode, and they can be selected by pressing a button located on the back of the instrument. A third mode, referred to as dark-viewing mode, allows measurement of the dark current for high and low gains. Thus the measurements of direct solar extinction and water-leaving radiance are made sequentially, not simultaneously, but the small time difference between the two types of measurements (see the measurement protocol in Subsection 2.C) is not a significant factor for satellite ocean-color evaluation. The internal memory (458 Mbytes) and the Ni–Cd batteries allow the instrument to be operated for three months in normal mode (i.e., measurements at the time of satellite overpass) without saturating the memory or needing to recharge the batteries. The parameters and variables stored in the internal memory are latitude, longitude, date, time, air pressure and temperature, radiance counts, and magnetometer and inclinometer angles. The data stored in the memory can be downloaded and the memory emptied at any time during a campaign in which specific personal computer software is used.

C. Measurement Protocol

The measurement protocol consists of making consecutive measurements in Sun-, sea-, and dark-viewing modes. In Sun- and sea-viewing modes data are acquired in 10 s; in dark-viewing mode, 20 s (10 s for each gain). A complete measurement sequence, therefore, can be made within 1 min. Repeating the measurement sequence several times is recommended to improve data quality. Each type of data file has the same format, facilitating data processing. In Sun-viewing mode the instrument is pointed toward the Sun and properly aligned by use of a finder (Fig. 3, top). Only the maximum value over 1 s is stored in Sun-viewing mode (10 values total), reducing experimental errors due to ship motion. In Sea-viewing mode the instrument is positioned at 45° from nadir and at 135° from the solar plane by use of the four light indicators (two for nadir angle, two for azimuth angle; see Fig. 3, bottom). In addition, the surface must be lit by direct sunlight. The operator has a choice of two azimuth positions at 135° from the Sun and selects the position that avoids shadows and ship wake. Onboard a ship the best measurements are generally obtained from the bow, upwind from exhaust fumes (the ship is usually in the wind when not steaming).

In addition to the data stored in the SIMBAD instrument memory, ancillary information about cloud type and coverage, barometric air pressure, wind speed, and surface state (wave height and direction, whitecaps) are logged by the operator for each measurement sequence. This information is necessary to correct the data for various perturbing effects and to control data quality (see Section 4).

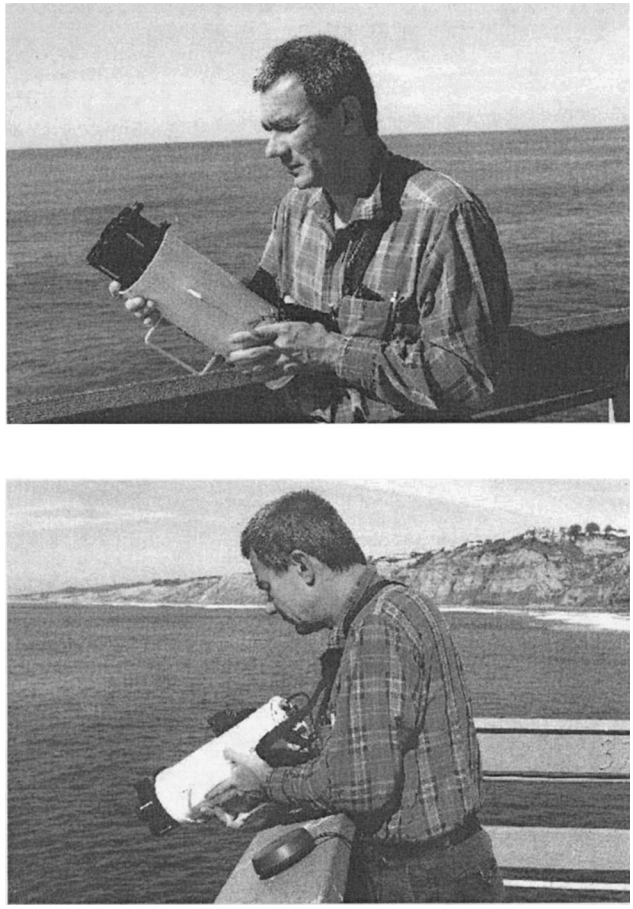

Fig. 3. R. Frouin making SIMBAD measurements of marine reflectance (top) and aerosol optical thickness (bottom) from the Scripps Institution of Oceanography pier in La Jolla, California. To measure marine reflectance, he points the instrument toward the ocean surface at a nadir angle of ~45° and an azimuth angle of 135° with respect to the Sun's principal plane. The instrument is secured with a cord. To measure aerosol optical thickness, he points the instrument toward the Sun with the help of a finder.

3. Radiometric Calibration

In the following equations the numerical count for Sun and sea measurements, *CN*, is considered to be corrected for dark current. The dark-current count, therefore, is omitted for clarity. These two measurements require different calibration methods, which are described below.

A. Sun-Viewing Mode

The instrument in Sun-viewing mode is calibrated by use of the Bouguer–Langley method. The calibration procedure consists of measuring the Sun intensity through a stable atmosphere as a function of air mass and extrapolating the measurements to zero air mass. After passing through the atmosphere, the

Sun intensity (irradiance) in spectral band i can be expressed as

$$I_i(\theta_s) = I_{0i}(d_0/d)^2 \exp[-\tau_i m(\theta_s)], \quad (1)$$

where I_{0i} is the extraterrestrial Sun irradiance in band i for the mean Earth–Sun distance d_0, θ_s is the Sun zenith angle, τ_i is the total optical thickness of the atmosphere in band i (assumed to be constant during the calibration), m is the air mass, and d is the Earth–Sun distance during the calibration. The I_{0i} values are obtained from Neckel and Labs,[31] m is computed as a function of θ_s following Kasten and Young,[32] and d is computed according to Paltridge and Platt.[33] Equation (1) is valid only in the absence of absorption by water vapor and minor gases.

During Sun-viewing mode, the measured numerical count in band i, CN_i, is proportional to I_i, allowing one to write

$$\ln(CN_i) = \ln(CN_{0i}) + 2\ln(d_0/d) - \tau_i m(\theta_s), \quad (2)$$

where CN_{0i} is the calibration coefficient for spectral band i. Therefore CN_{0i} is obtained by plotting the CN_i values as a function of air mass and by extrapolating to zero air mass or, more accurately, by regressing $\ln(CN_i)$ versus m. The measurements are performed under the clearest conditions possible (e.g., at a high-altitude site) to minimize the effects of a variable atmosphere.

B. Sea-Viewing Mode

The instrument in sea-viewing mode is calibrated by use of an integrating sphere, whose output spectral radiance is calibrated with equipment and methods that are traceable to the National Institute of Standards and Technology and that are further controlled in radiometric intercomparison activities (e.g., see Refs. 34 and 35). The equivalent radiance of the sphere in band i, L_{si}, is first computed as follows:

$$L_{si} = \left[\int_i L(\lambda)R(\lambda)\mathrm{d}\lambda\right] \Big/ \left[\int_i R(\lambda)\mathrm{d}\lambda\right], \quad (3)$$

where λ is wavelength, L is the radiance delivered by the sphere, R is the spectral response of the SIMBAD instrument, and the integral is over the spectral range of band i. Because the numerical counts that are measured by the instrument placed in front of the sphere are proportional to the sphere radiance, the calibration coefficient for band i, K_i, is then given by

$$K_i = L_{si}/CN_i. \quad (4)$$

The integrating sphere is also used to measure the radiometric noise of the instrument at various radiance levels. For realistic radiance levels and the five spectral bands, the noise is fairly constant at $\sim 2 \times 10^{-5}$ when expressed in reflectance. Note that complementary calibrations can be made for multitemporal control during the campaign by using, for example, a Spectralon plaque.

4. Data Processing

A. Aerosol Optical Thickness and Angström Coefficient

To deduce aerosol optical thickness from the measurements in Sun-viewing mode, one must first compute the total optical thickness of the atmosphere τ_i by inverting Eq. (2):

$$\tau_i = [\ln(CN_{0i}) + 2\ln(d_0/d) - \ln(CN_i)]/m(\theta_s). \quad (5)$$

The total optical thickness, τ_i, is then corrected for molecular scattering and gaseous absorption, due mostly to ozone. This gives the aerosol optical thickness in band i, τ_{ai} as

$$\tau_{ai} = \tau_i - \tau_{ri}(P) - \tau_{oi}(U_o), \quad (6)$$

where τ_{ri} and τ_{oi} are the Rayleigh and ozone optical thickness in band i, respectively. The Rayleigh optical thickness depends on surface air pressure, P. It is computed by use of a depolarization factor of 0.0279.[7,8] The ozone contribution is computed from the vertically integrated ozone amount, U_o, obtained from climatology (see Ref. 36) or derived from Total Ozone Mapping Scanner observations.

The Angström coefficient, α, defined by the law $\tau_a(\lambda) \approx \lambda^{-\alpha}$, is determined by regressing on a log–log scale τ_{ai} versus the equivalent wavelength of band i, λ_i, by using the instrument's five spectral bands. The determination of α is more difficult at low-aerosol optical thickness simply because the uncertainty on τ_{ai} is rather constant in absolute value but becomes increasingly large in relative value as τ_{ai} decreases.

B. Total Atmospheric Transmittance

The total (i.e., direct plus diffuse) atmospheric transmittance in spectral band i, T_i, needs to be estimated to normalize the water-leaving radiance measurements into reflectance. It can be expressed (e.g., Ref. 37) as the product of the transmittance due to gaseous absorption, mostly of ozone, T_{oi}, and the transmittance due to molecular and aerosol scattering (including aerosol absorption), T_{rai}. We have

$$\begin{aligned} T_i(\theta_s) &= T_{oi}(\theta_s, U_o)T_{rai}(\theta_s, \tau_{ri}, \tau_{ai}) \\ &= \exp[-k_{oi}U_o m(\theta_s)]T_{rai}(\theta_s, \tau_{ri}, \tau_{ai}), \end{aligned} \quad (7)$$

where T_{oi} is explicited and k_{oi} is the ozone absorption coefficient in band i. The transmittance T_{rai} is computed by use of a radiative transfer model based on the successive orders of scattering method[38] with θ_s, τ_{ri}, and τ_{ai} as variable input. The effect of aerosol type on T_{rai} is small[39] and can be neglected. Alternatively, the analytical approximation proposed by Tanré *et al.*[39] can be used:

$$T_{rai}(\theta_s) = \exp[-(0.52\tau_{ri} + 0.16\tau_{ai})m(\theta_s)]. \quad (8)$$

Using this formula to estimate photosynthetically available radiation at the ocean surface, Frouin *et al.*[40] reported root-mean-squared differences of 4.7% in comparison with *in situ* measurements. Computing T_{rai} by means of the radiative transfer model of Deuzé *et al.*[38] or Eq. (8) is valid only under clear-sky

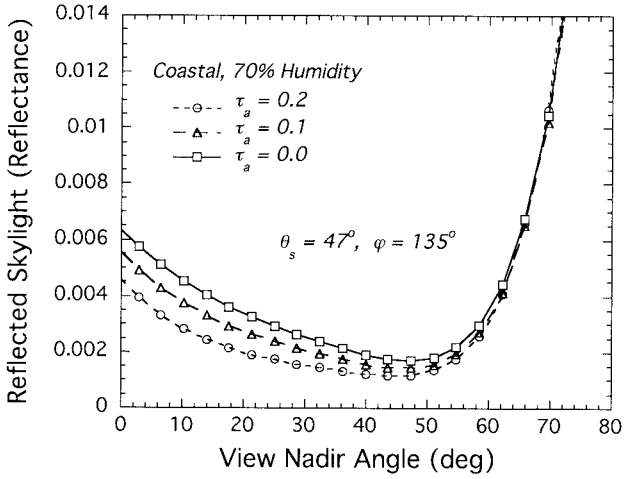

Fig. 4. Parallel-polarized reflectance of the ocean at 443 nm for a solar zenith angle of 47°, a relative azimuth angle of 135°, a wind speed of 5 m s^{-1}, and assuming a water-body reflectance of zero.[25] The atmosphere contains molecules and coastal aerosols (C70 model from Ref. 9) of varied optical thicknesses.

conditions (no clouds). The extended use of the SIMBAD radiometer to any kind of cloudy conditions would be interesting for developing and verifying bio-optical algorithms but would require a simultaneous measurement of downwelling irradiance.

C. Marine Reflectance

Because the variable of interest is diffuse marine reflectance, defined as radiance times π and divided by the extraterrestrial solar irradiance, the polarized reflectance in spectral band i measured by viewing the surface (sea-viewing mode), ρ_{ui}, is obtained from the recorded numerical count by using the following formula:

$$\rho_{ui} = \pi K_i C N_i (d/d_0)^2 / I_{0i} \cos(\theta_s). \quad (9)$$

As indicated in Section 2, ρ_{ui} should be measured in a specific viewing geometry, i.e., at a nadir angle of 45° and at an azimuth angle of 135° with respect to the Sun, in order to minimize skylight reflection effects. The inclinometer and magnetometer angles are used to select the optimum viewing geometry. Measurements made at a nadir angle outside the range 45° ± 5° and at a relative azimuth angle outside the range 135° ± 10° are not processed.

The reflectance ρ_{ui} is then corrected for residual skylight and atmospheric transmittance to yield the vertically polarized diffuse water reflectance, ρ_{wi}'. We have

$$\rho_{wi}' = (\rho_{ui} - \rho_{0i})/T_i, \quad (10)$$

where ρ_{0i} is the reflectance due to skylight reflection in spectral band i. This reflectance is computed accurately from the molecular optical thickness, the aerosol optical thickness and type (i.e., Angström coefficient), and the surface wind speed, according to Fougnie *et al.*[25] Figure 4 shows ρ_0 as a function of nadir angle for a Sun zenith angle of 47°, a relative azimuth angle of 135°, a wavelength of 443 nm, and a wind speed of 5 m s^{-1}. The atmosphere contains molecules and coastal aerosols of varied optical thicknesses (C70 aerosol model from Ref. 9). During viewing at 45° from nadir, the skylight contribution is of the order of 0.002 (in reflectance units). Note that, because the surface is not flat, the minimum value of ρ_0 is not obtained at exactly the Brewster angle (53°), but at a smaller angle (45°). The case displayed in Fig. 4, with a Sun zenith angle close to the 45° view nadir angle, is not a special case. Results for other wavelengths, solar zenith angles, and aerosol types can be found in Fougnie *et al.*[25]

The radiometric measurements might be contaminated by whitecaps caused by wind action on the surface or by foam and bubbles generated by the ship or by residual glitter. Sunlight scattered by clouds may also be reflected by the surface in the instrument's field of view. To remove these unwanted effects, we examine the reflectance measured in the spectral band centered at 870 nm ($i = 5$), ρ_{u5}. First, a threshold, typically 0.001, is applied to ρ_{u5} to eliminate the most perturbed measurements. Second, $\rho_{ui}(i = 1, \ldots, 4)$ is corrected by using ρ_{u5} and by assuming that the extra reflectance due to whitecaps, clouds, etc., does not depend on wavelength in the spectral range 443–870 nm. With this additional correction, $\rho_{wi}'(i = 1, \ldots, 4)$ becomes

$$\rho_{wi}' = (\rho_{ui} - \rho_{0i})/T_i - (\rho_{u5} - \rho_{05})/T_5, \quad i = 1, \ldots, 4. \quad (11)$$

Thus only ρ_{wi}' in spectral bands 1–4, i.e., the bands centered at 443, 490, 560, and 670 nm, respectively, is obtained after correction. Equation (11) can be applied effectively because the radiometric measurements are acquired simultaneously in the instrument's five spectral bands (cloud effects strongly depend on surface-wave slope, and whitecaps may be changing quickly with time). On the other hand, treating whitecaps as gray bodies, even though they are not white spectrally[41–43] is sufficient because only the less-perturbed measurements are selected. Over turbid coastal waters, the diffuse reflectance is not null at 870 nm; consequently, Eq. (11) is not valid for those waters.

Molecules and hydrosols polarize the light scattered by the water body. Because the SIMBAD measurements are made through a vertical polarizer, polarization effects must be corrected to yield the total water reflectance. If γ_i denotes the ratio of vertically polarized reflectance to total reflectance in spectral band i, we have

$$\rho_{wi} = 2\gamma_i \rho_{wi}', \quad (12)$$

where ρ_{wi} is the water reflectance in spectral band i. The factor 2 in Eq. (12) is introduced because the radiometric calibration is based on the total radiance of the integrating sphere [see Eq. (5)], and this radiance is twice the radiance measured through the polarizer. In other words, $\gamma_i = 0.5$ for unpolarized

light. For the viewing geometry considered, and because of refraction at the air–sea interface, the underwater scattering angle is generally large, i.e., in the range 145°–160°. In a scattering geometry such as this, polarization by the water body is small, typically 10% (e.g., see Ref. 44), and would be null if the scattering angle were 180°. A crude estimate of γ_i was obtained by Fougnie *et al.*[25] under the assumption that polarization is due only to water molecules, i.e., γ_i varies between 0.41 and 0.47.

More accurate computations of γ_i were performed by use of the Monte Carlo method for a realistic ocean–atmosphere system containing molecules, aerosols, and hydrosols. The ocean surface was wavy, with the wave slope determined according to Cox and Munk.[45] It was assumed that hydrosols were spherical phytoplankton particles. Their characteristics (size distribution and refractive index) were specified according to Morel *et al.* and Aas.[46–48] Mie theory was used to compute the scattering matrix and the scattering and absorption cross sections. To calibrate the theoretical results, we adjusted the volume number concentration so that the computed scattering coefficient matched the parameterization of Morel.[12] Varied volume number concentrations, thus pigment concentrations, were considered. The polarization signature of downwelling radiance at the surface, due to air molecules and aerosols, was also taken into account.

Figure 5(a) displays γ versus the nadir angle for three types of phytoplankton particles. The Sun zenith angle is 30°, the relative azimuth angle is 129.4°, the wavelength is 450 nm, the aerosols are of oceanic type,[49] with an optical thickness of 0.2, and the wind speed is 5 m s^{-1}. The phytoplankton particles have a radius between 0.2 and 50 μm that is distributed according to a Junge law (exponent of -3.6), and their refractive index is $1.03 - 0.001i$ (Type 1), $1.10 - 0.00001i$ (Type 2), and $1.15 - 0.00001i$ (Type 3). Pigment concentration is 0.1 mg m^{-3}. At a nadir angle of 45°, γ is ~0.44 and varies little (to within ± 0.01) with phytoplankton type. Figure 5(b) shows that, for phytoplankton Type 2, γ increases with pigment concentration, from ~0.43 at 0.01 mg m^{-3} to 0.48 at 10 mg m^{-3}. Other simulations (not presented here) indicate an increase of γ with Sun zenith angle to 0.48 at 60° as well as a small dependence with wavelength (i.e., a few 0.01) in the spectral range of interest. The Monte Carlo results agree with measurements made by a scanning polarization radiometer.[50] Thus polarization effects by the water body can be corrected to ~2% from the Sun zenith angle and pigment concentration, which can be estimated from ρ_{w1}'/ρ_{w3}' or ρ_{w2}'/ρ_{w3}'.

The data processing is illustrated in Fig. 6, which displays the measured polarized reflectance ρ_{ui} [Fig. 6(a)] and the final water reflectance ρ_{wi} [Fig. 6(b)] for a selected sea-viewing file. The data were collected on 29 January 1999 at 4.04 °S and 18.18 °W during the Aerosols-99 campaign. The solar zenith angle was 41.8°, the wind speed was 6.3 m s^{-1}, and the sky was completely free of clouds. After correction of the

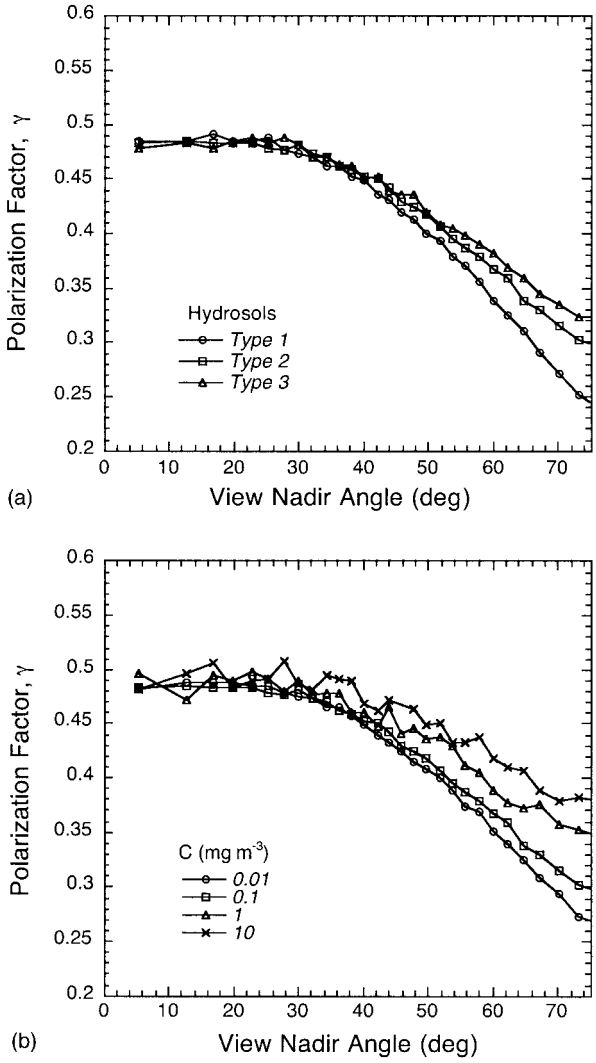

Fig. 5. Polarization factor γ versus view nadir angle for (a) three types of phytoplankton particles and a pigment concentration of 0.1 mg m^{-3} versus (b) pigment concentration for particles of Type 2.

perturbing effects, the variability in ρ_u is reduced over the 10-s measurement period (i.e., 100 samples), and ρ_{wi} is slightly lower than ρ_{ui} (by less than 0.001). The correction of residual skylight, which decreases ρ_{ui}, is partly compensated for by the correction of polarization effects, which increases ρ_{ui}. The total correction is relatively small, except in spectral bands 3 and 4, which exhibit a low signal (i.e., the radiometer almost measures the desired variable). This is a definite advantage over underwater techniques, which require extrapolation of radiometric measurements to the surface. The average water reflectance over the 10-s measurement period is 0.0214 ± 0.0006, 0.0195 ± 0.0006, 0.0048 ± 0.0002, and 0.00014 ± 0.00010 in spectral bands 1–4, respectively. Because of surface waves, the radiometer may not always be positioned at a nadir angle of 45° with respect to the direction normal to the surface, causing fluctuations in the measured signal. Reflected light

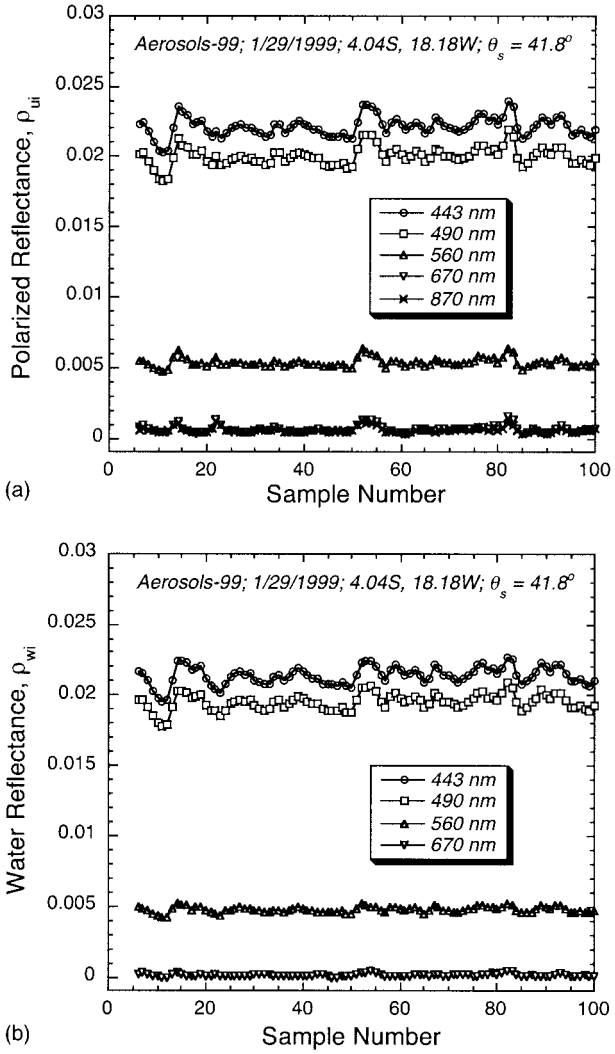

Fig. 6. (a) Measured polarized and (b) final water reflectance for a sea-viewing file corresponding to data collected on 29 January 1999 at 4.04 °S and 18.18 °W during the Aerosols-99 campaign. The solar zenith angle was 41.8°, the wind speed was 6.3 m s^{-1}, and the sky was completely free of clouds.

will pass through the vertical polarizer when the instrument is not properly oriented; i.e., the measurements will exhibit higher reflectance. This effect, conspicuous in spectral bands 1 and 2, can be corrected by selection of the smallest values in the time series.

5. Error Budget

A. Atmospheric Variables

In Sun-viewing mode the SIMBAD radiometer works like a classic sunphotometer, for which the inaccuracy of the retrieved aerosol optical thickness has previously been evaluated (e.g., see Ref. 16). This inaccuracy is due chiefly to errors on the calibration coefficient, the Rayleigh optical thickness, and the ozone optical thickness [see Eqs. (5) and (6)]. From Bougley–Langley plots obtained during several years at Stevenson Peak (1896-m altitude) in the Mount Laguna Mountains, California, the error on the calibration coefficient, $\Delta[\ln(CN_{0i})]$, is estimated at ±0.02, ±0.02, ±0.015, ±0.01, and ±0.01 in spectral bands 1–5, respectively. The error on the Rayleigh optical thickness, $\Delta\tau_{ri}$, is due to computational uncertainty (i.e., ±1% at standard pressure) and to uncertainty on pressure (i.e., ±10 hPa, conservatively), translating into ±0.005, ±0.004, ±0.002, ±0.001, and negligible in spectral bands 1–5, respectively. The error on the ozone optical thickness, $\Delta\tau_{oi}$, significantly affects spectral bands 3 and 4 (centered at 560 and 670 nm) and is attributed to the uncertainty in the vertically integrated ozone amount, i.e., ±10%, which gives errors of ±0.010 and ±0.004, respectively. Note that the error on the calibration coefficient affects the inaccuracy of the aerosol optical thickness in a manner inversely proportional to air mass [Eq. (5)]. Estimates of aerosol optical thickness are more accurate when observations are made at larger Sun zenith angles.

Table 2. Inaccuracy of the SIMBAD Aerosol Optical Thickness ($m = 1$)

	Wavelength (nm)				
Error Type	443	490	560	670	870
$\Delta\ln(CN_0)$	±0.020	±0.020	±0.015	±0.01	±0.01
$\Delta\tau_r$	±0.005	±0.004	±0.002	±0.001	—
$\Delta\tau_o$ [a]	—	—	±0.010	±0.004	—
$\Delta\tau_a$ (quadratic)	±0.021	±0.020	±0.018	±0.011	±0.010

[a] τ_o is the optical zone thickness, k_oU_o.

The various errors are summarized in Table 2, which also gives the resulting quadratic inaccuracy of τ_{ai} at zero air mass, $\Delta\tau_{ai}$, as ±0.021, ±0.020, ±0.018, ±0.011, and ±0.010 in spectral bands 1–5, respectively. Most of the inaccuracy is due to error in the calibration coefficient. The absolute inaccuracy of τ_{ai} does not depend on τ_{ai}. Thus the relative inaccuracy varies as $1/\tau_{ai}$ and is large when τ_{ai} is small (e.g., 40% in spectral band 1 when $\tau_{ai} = 0.05$). The above inaccuracy values do not take into account the error due to the size of the instrument's field of view (3°). Not only direct sunlight is measured, but also some light scattered by the atmosphere, resulting in τ_{ai} estimates that are biased low. The effect is small for continental aerosols, with values of 0.002 and 0.001 in spectral bands 1 and 5, respectively, when τ_{ai} is equal to 0.1, but may be 5–10 times larger for maritime aerosols whose phase function exhibits a much higher forward peak. A correction can be made by use of the Angström coefficient (i.e., the aerosol model) obtained from the measurements.

The inaccuracy of the Angström coefficient α reflects the inaccuracy of the aerosol optical thickness τ_{ai}. It decreases with increasing τ_{ai} and α. Using Table 2 and obtaining α by linearly fitting τ_{ai} versus λ_i on a log–log scale, the inaccuracy of α is approximately ±0.19 and ±0.33 when $\tau_{a5} = 0.1$ and $\alpha = 1.5$ and 0, respectively. The values decrease to ±0.10 and ±0.16 when $\alpha = 0.2$. Over the open ocean, τ_{ai} and α are often small (i.e., $\tau_{a5} < 0.05$ and $\alpha \approx 0$),

Table 3. Inaccuracy of the SIMBAD Diffuse Marine Reflectance

Error Type	Wavelength (nm) 443	490	560	670
$NE\Delta\rho_u$	±0.00004	±0.00004	±0.00004	±0.00004
$\Delta_c\rho_u$	±0.00121	±0.00092	±0.00023	±0.00003
$\Delta_t\rho_w$	±0.00027	±0.00019	±0.00004	±0.00001
$\Delta_s\rho_w$	±0.00042	±0.00035	±0.00028	±0.00015
$\Delta_p\rho_w$	±0.00048	±0.00037	±0.00009	±0.00001
$\Delta\rho_w$ (quadratic)	±0.00139 (5.7%)	±0.00107 (5.7%)	±0.00037 (7.8%)	±0.00016 (22.8%)

making it difficult to estimate α accurately. In such conditions, however, the atmospheric correction of satellite ocean color is not a difficult problem.

Taking into account the above uncertainty on Rayleigh optical thickness (approximately ±2%), aerosol optical thickness (Table 2), and ozone amount (±10%), the inaccuracy of the atmospheric transmittance T_i can be estimated. It is ~0.7% in spectral bands 1–3 and 0.4% and 0.2% in spectral bands 4 and 5, respectively, when $\tau_{a5} = 0.1$, $\alpha = 1$, and the Sun is at zenith. The values increase with aerosol optical thickness and Sun zenith angle. They become 1.6%, 0.8%, and 0.4% when the Sun zenith angle is 60°. The coefficient 0.16 in Eq. (8) may vary with aerosol type, but the consequence on the inaccuracy of T_i is negligible.

B. Marine Reflectance

Table 3 displays, for a typical case, the various errors contributing to the inaccuracy of the marine reflectance ρ_{wi} and the resulting quadratic inaccuracy, $\Delta\rho_{wi}$. The Sun zenith angle is 60°, the aerosol optical thickness is 0.1 in spectral band 5, the aerosol model is C70,[9] the phytoplankton pigment concentration is 0.1 mg m^{-3} (case 1 waters), and the wind speed is 7.5 m s^{-1}. The noise-equivalent reflectance, $NE\Delta\rho_{ui}$, is $\pm 4 \times 10^{-5}$, which is twice the value given in Table 1 because the air mass is equal to 2. The uncertainty in the radiometric calibration, in fact the sum of the uncertainty on the calibration of the integrating sphere and the uncertainty on the spectral solar irradiance, is typically ±5%. This introduces an error, $\Delta_c\rho_{ui}$, of $\pm 12.1 \times 10^{-4}$, $\pm 9.2 \times 10^{-4}$, $\pm 2.3 \times 10^{-4}$, and $\pm 0.3 \times 10^{-4}$ in spectral bands 1–4, respectively. The uncertainty on atmospheric transmittance, estimated at ±1% for the same bands, yields an error $\Delta_t\rho_{wi}'$ of 2.7×10^{-4}, 1.9×10^{-4}, 0.4×10^{-4}, and 0.1×10^{-4}, respectively. The error due to uncertainty in the correction of residual skylight reflection, $\Delta_s\rho_{wi}'$, is computed with an assumed uncertainty of ±2 m s^{-1} on wind speed, ±0.01 on aerosol optical thickness in spectral band 5, ±5° on the viewing nadir angle, and ±10° on the relative azimuth angle, giving values of $\pm 4.2 \times 10^{-4}$, $\pm 3.5 \times 10^{-4}$, $\pm 2.8 \times 10^{-4}$, and $\pm 1.4 \times 10^{-4}$, respectively. The error due to uncertainty in the correction of whitecap and cloud effects [Eq. (11)] is neglected. Finally, uncertainty in the polarization factor γ_i (~2%; see Subsection 4.C) translates into an error, $\Delta_p\rho_{wi}$, of $\pm 4.8 \times 10^{-4}$, $\pm 3.7 \times 10^{-4}$, $\pm 0.9 \times 10^{-4}$, and $\pm 0.1 \times 10^{-4}$, respectively. Summing the individual errors squared, the resulting $\Delta\rho_{wi}$ is $\pm 13.9 \times 10^{-4}$, $\pm 10.7 \times 10^{-4}$, $\pm 3.7 \times 10^{-4}$, and $\pm 1.6 \times 10^{-4}$ or ±5.7%, ±5.7% ±7.8% and ±22.8% of the marine reflectance in spectral bands 1–4, respectively. The inaccuracy of ρ_{w1} and ρ_{w2} results essentially from the uncertainty in the radiometric calibration coefficients. Imperfect correction of skylight reflection (already minimized by the vertical polarizer) has a small effect on the inaccuracy in spectral bands 1 and 2, but it contributes significantly to the inaccuracy of ρ_{w3} and dominates the inaccuracy of ρ_{w4}.

Note that the error budget discussed above does not include the effect of the platform from which the measurements are made and whose presence generally increases the amount of light reflected by the surface into the instrument's field of view as well as the downward solar irradiance. In a typical experimental configuration, the surface must have a slope of at least 45° for the instrument to measure the light reflected from the platform. The probability of having such a slope is very small for wind speeds at which SIMBAD measurements are made (<15 m s^{-1}),[45] and the resulting increase in measured reflectance is negligible. The effect on downward solar irradiance is not significant, even when the platform structures are totally reflective (albedo of 1). When viewing the ocean surface at an azimuth angle of 135° from the Sun, the side of the platform from which the measurements are made is either in the shade or lit by the Sun at a very oblique angle. Consequently, the effective albedo of the structures is small, increasing downward solar irradiance typically by a fraction of 1%.

6. Experimental Verification

A. Aerosol Optical Thickness

To evaluate the aerosol optical thickness derived from SIMBAD measurements, we performed a comparison by using another sunphotometer during ACE-2. This sunphotometer, known as AATS-6, tracks the Sun automatically and measures direct solar extinction in six spectral bands.[51] The field of view is 2.2° (half-angle). During ACE-2 the spectral bands were centered at 380, 451, 525, 863, 941, and 1021 nm. Data processing, including removal of measurements contaminated by clouds and shipboard structures, is described by Livingston *et al.*[52] The aerosol optical thickness from AATS-6 was linearly interpolated to the SIMBAD spectral bands on a log–log scale. The comparison between SIMBAD and AATS-6 measurements was performed during three days (i.e., 24, 25, and 30 June 1997). Varied aerosol conditions (i.e., optical thickness in the range 0.02–0.3 and Angström coefficient in the range 0.15–1.30) were encountered. The agreement is good between measurements made by the two instruments (Fig. 7 and Table 4). For optical thickness, the mean difference is between −0.01 and 0.02, depending on

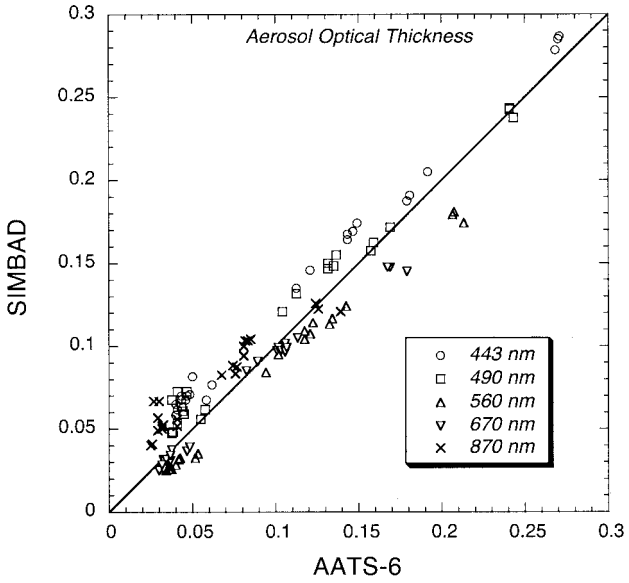

Fig. 7. Comparison of aerosol optical thickness derived from three days of measurements made by the SIMBAD radiometer and by the AATS-6 sunphotometer[51] during ACE-2 (23 matchups).

wavelength, and the root-mean-squared difference is 0.01 or less. For the Angström coefficient, the values are −0.07 and 0.15, respectively. These correlation statistics are consistent with the inaccuracy discussed in Subsection 5.A. A useful index to isolate small particles (e.g., pollution-type aerosols) is the product of the optical thickness in spectral band 5 and the Angström coefficient. Estimates of this index made by the two instruments agree to within ±0.01 (Table 4). Other comparisons were made with a Prede radiometer during a CalCOFI cruise[53] and with Microtops and shadow-band radiometers during the Aerosols-99 Experiment.[54] These comparisons also showed agreement (i.e., average differences of 0.02–0.03 at 500 nm) between the aerosol optical thickness measured by SIMBAD and that made with the other instruments.

B. Marine Reflectance

The marine reflectance derived from the SIMBAD measurements in sea-viewing mode was compared with that derived from the underwater measurements of upward radiance and downward irradiance during four CalCOFI cruises, CalCOFI-9610 (October 1996), CalCOFI-9710 (October 1997), CalCOFI-9802 (February 1998), and CalCOFI-9804 (April 1998), and during the Aerosols-99 Experiment (January–February 1999). The CalCOFI cruises were conducted off the California coast in clear and turbid waters. The Aerosols-99 Experiment occurred along a route from Norfolk, Virginia, to Cape Town, South Africa, and Port Louis, Mauritius. Waters with varied optical properties were sampled in regions of the Gulf Stream, in subtropical gyres, in South Equatorial currents, and in the Aghulas Current.

The underwater measurements were made by an integrated profiling system, including a Multiwavelength Environmental Radiometer Model 2040 (MER-2040) manufactured by Biospherical Instruments, Incorporated. The radiometer acquired vertical profiles of downward irradiance, $E_d(Z)$, and upward radiance, $L_u(Z)$, in spectral bands centered at 380, 395, 443, 455, 490, 510, 532, 555, 570, and 665 nm. The MER-2040 unit was deployed from the A-frame on the ship's stern at each station according to SeaWiFS protocols.[14] The E_d and L_u values were extrapolated to the zero depth ($Z = 0^-$) according to Mitchell and Kahru.[55] Shelf-shadowing effects were corrected with the scheme recommended by Gordon and Ding and by Mueller and Austin.[14,56] Normalized radiance just below the surface, $L_u(0^-)/E_d(0^-)$, was transformed into normalized radiance just above the surface, $L_u(0^+)/E_d(0^-)$, using the factor 0.529 (e.g., see Morel and Mueller[57]). Marine reflectance ρ_w was computed as $\pi L_u(0^+)/E_d(0^+)$. In addition to the L_u and E_d measurements, water was sampled at selected depths with a separate conductivity, temperature, and depth rosette system. The chlorophyll a and phaeopigment concentrations of the water samples were determined by the fluorometric method.[58]

Figure 8 presents a scatter plot of the marine reflectance obtained from SIMBAD and MER measurements for the SIMBAD spectral bands centered at 443, 490, 560, and 670 nm (bands 1–4). To estimate the MER values in SIMBAD spectral band 3, a linear interpolation was made between the MER measurements in the spectral bands centered at 555 and 570 nm. Effects due to different viewing geometry (MER measures at nadir and SIMBAD at 45° from nadir) were not corrected. A total of 36 matchups are used for spectral bands 1 and 3, but only 21 matchups for spectral bands 2 and 4. During the CalCOFI-9610 cruise the SIMBAD radiometer did not measure in band 2 and look-up tables that are necessary for the data processing of band 4 were not

Table 4. Comparison Statistic of Aerosol Optical Thickness, τ_a, at 443, 490, 560, 670, and 870 nm, Angström Coefficient, α, and Aerosol Index, $\tau_a(870)\alpha$, Derived from Measurements by the SIMBAD Radiometer and the AATS-6 Sunphotometer during ACE-2[a]

Statistic	$\tau_a(443)$	$\tau_a(490)$	$\tau_a(560)$	$\tau_a(670)$	$\tau_a(870)$	α	$\alpha\tau_a(870)$
Bias	0.0196	0.0121	−0.0145	−0.0068	0.0155	−0.0709	−0.0073
RMSD	0.0062	0.0099	0.0078	0.0084	0.0118	0.1555	0.0052
R	0.9951	0.9854	0.9906	0.9808	0.9156	0.7787	0.9891
N	23	23	23	23	23	23	23

[a]RMSD is the root-mean-squared difference, R is the correlation coefficient, and N is the number of matchups. A positive bias signifies a higher SIMBAD value.

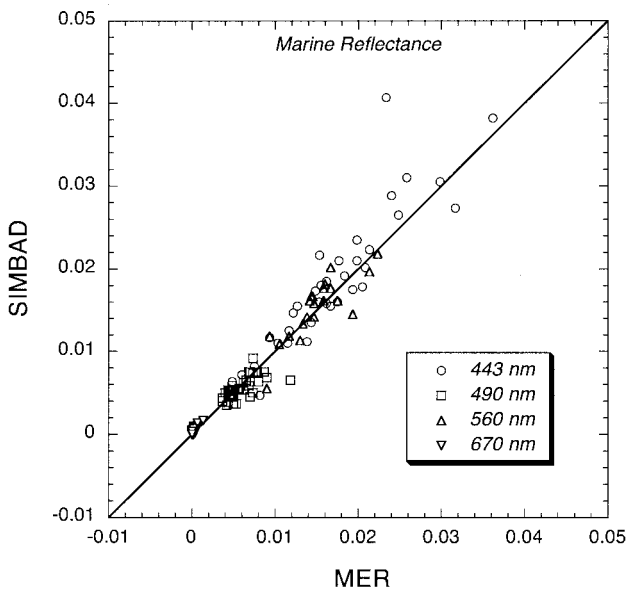

Fig. 8. Comparison of marine reflectance derived from SIMBAD and MER measurements obtained during the CalCOFI and Aerosols-99 cruises: 36 matchups for 443 and 560 nm, and 21 matchups for 490 and 670 nm.

generated (see Subsection 4.C). For these matchups the Sun zenith angle was mostly less than 60° and the fractional cloud coverage was less than 0.2. Figure 9 displays marine reflectance versus pigment concentration (chlorophyll a + phaeophytin a) for the two types of instrument and each of the four spectral bands indicated above. In the figure the relation between marine reflectance and pigment concentration predicted by the bio-optical model of Morel[12] is plotted for reference. The marine reflectance from SIMBAD and MER are in general agreement (Fig. 8). At 443 nm the SIMBAD values are higher by 5.0%, but at 490 and 560 nm they are biased low by 0.8 and 9.1%, respectively (Table 5). For these three wavelengths, the normalized root-mean-squared difference is in the range 13%–23%. At 670 nm the SIMBAD values are, on average, higher by a factor of 0.76, and the root-mean-squared difference is relatively large (i.e., 90%; Table 5); however, the radiometric signal, thus the absolute difference, is small.

The comparison statistics between SIMBAD- and MER-derived marine reflectances are difficult to explain quantitatively because of the limited number of

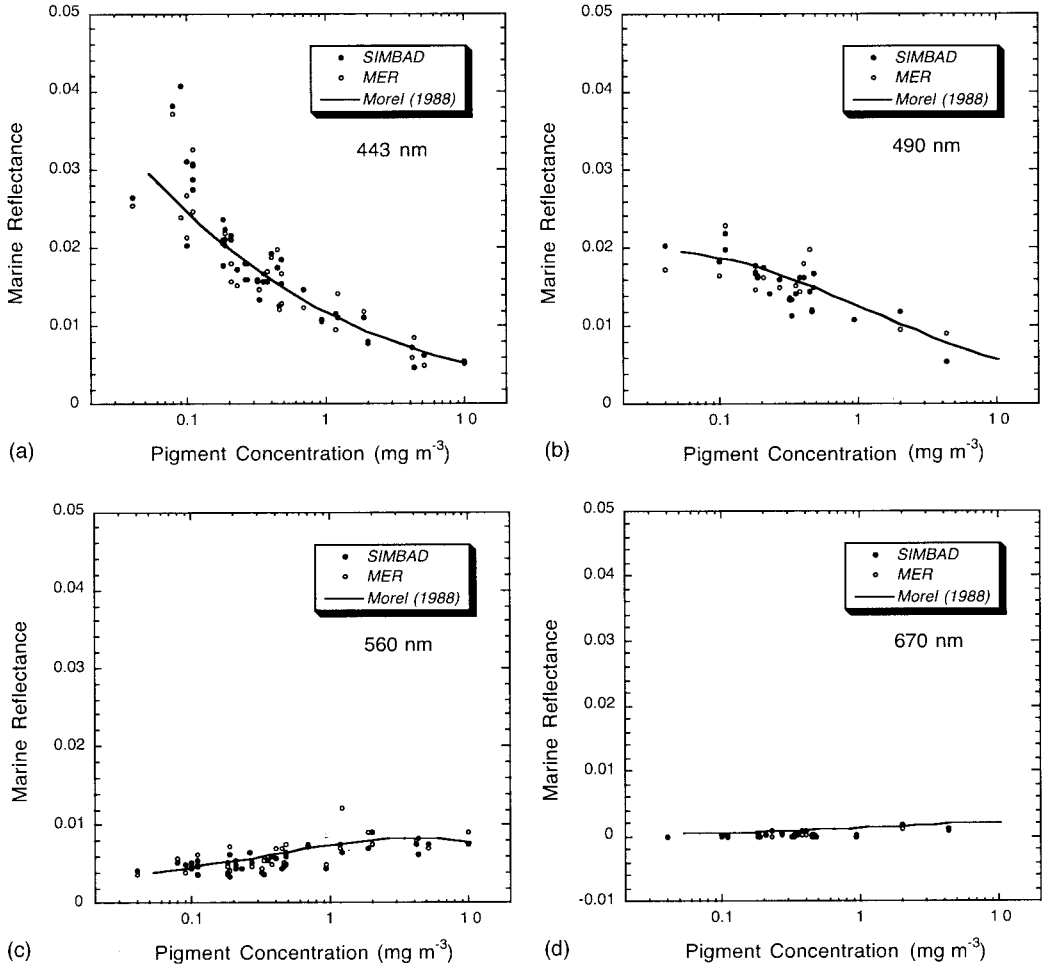

Fig. 9. Marine reflectance derived from SIMBAD and MER measurements at (a) 443 nm, (b) 490 nm, (c) 560 nm, and (d) 670 nm versus the pigment concentration estimated from water samples with the fluorometric method. The solid line represents the relation between marine reflectance and pigment concentration that is predicted by the bio-optical model of Morel.[12]

Table 5. Comparison Statistic of Marine Reflectance Derived from SIMBAD and MER-2040 Radiometer Measurements during CalCOFI and Aerosols-99 Cruises[a]

Statistic	$\rho_w(443)$	$\rho_w(490)$	$\rho_w(560)$	$\rho_w(670)$
Mean	0.01781	0.01532	0.00581	0.00044
Bias	0.00089	−0.00013	−0.00053	0.00024
	(5.0%)	(−0.8%)	(−9.1%)	(75.9%)
RMSD	0.00354	0.00202	0.00132	0.00029
	(19.8%)	(13.2%)	(22.8%)	(90.5%)
R	0.9083	0.8354	0.6808	0.7780
N	36	21	36	21

[a]RMSD is the root-mean-squared difference, *R* is the correlation coefficient, and *N* is the number of matchups. A positive bias signifies a higher SIMBAD value.

matchups. They may be attributed to several factors: (1) inaccuracy of the SIMBAD measurements; (2) environmental variability (e.g., MER measurements are made from the ship's stern and SIMBAD measurements from the bow); (3) bidirectional characteristics of the marine reflectance, which, since ignored, may affect differences by ±10%[59]; (4) different spectral responses of the SIMBAD and MER instruments, a critical issue in the blue wavelength, where solar irradiance is variable spectrally; and (5) inaccuracy of the MER measurements, typically of the order of ±12–24%.[30] Note that applying the average bidirectional factors of Morel and Mueller[57] to account for the different viewing geometry of the SIMBAD and MER measurements does not substantially modify the comparison statistics. The total normalized root-mean-squared difference (i.e., including the bias) changes from 20.5% to 21.3% at 443 nm, 13.2% to 15.5% at 490 nm, 24.6% to 17.5% at 560 nm, and 118% to 115% at 670 nm (i.e., only decreases significantly at 560 nm). Improvement is probably masked by more important effects, but uncertainty in the bidirectional factors, which assume certain optical properties for the hydrosols (e.g., scattering phase function), could have introduced additional noise. In view of these sources of uncertainty, the comparison statistics are consistent with the SIMBAD theoretical inaccuracy, except at 670 nm (Section 4 and Table 5). On the other hand, the marine reflectance obtained by both types of instruments is in reasonable agreement with predictions of the bio-optical model over the entire range of measured pigment concentration, except below 0.1 mg m^{-3} (Fig. 9). In such oligotrophic waters, the inaccuracy of the pigment concentration (typically 0.02–0.03 mg m^{-3}) is relatively large. The SIMBAD-derived marine reflectance at 670 nm increases with pigment concentration, as suggested by the bio-optical model, whereas the MER values exhibit much less sensitivity [Fig. 9(d)], giving confidence in the SIMBAD data processing.

Table 6. Comparison Statistic of Three Bio-optical Indices Computed with Marine Reflectance Derived from SIMBAD and MER Measurements (Table 4)[a]

Statistic	$\rho_w(443)/\rho_w(560)$	$\rho_w(490)/\rho_w(560)$	NDPI
Bias	0.405	0.262	0.001
	(11.7%)	(8.4%)	(0.2%)
RMS	0.744	0.426	0.172
D	(21.6%)	(13.7%)	(22.0%)
R	0.9359	0.9117	0.8859
N	36	21	21

[a]RMSD is the root-mean-squared difference, *R* is the correlation coefficient, and *N* is the number of matchups. A positive bias signifies a higher SIMBAD value. NDPI[60] is defined as the normalized difference $[\rho_w(443) - \rho_w(560)]/\rho_w(490)$.

Satellite-derived ocean color generally provides surface chlorophyll *a* or pigment concentration information. This variable is estimated by using simple ratios of marine reflectance in the blue and green [e.g., Ref. 13] or more complex indices, such as the Normalized Difference Phytoplankton Index (NDPI).[60] Table 6 displays comparison statistics for ρ_{w1}/ρ_{w3}, ρ_{w2}/ρ_{w3}, and $(\rho_{w1} - \rho_{w3})/\rho_{w2}$ (NDPI) obtained from the SIMBAD and MER data sets. The bias is similar for ρ_{w1}/ρ_{w3} and ρ_{w2}/ρ_{w3} (11.7% and 8.4%, respectively), but the root-mean-squared difference is substantially lower for ρ_{w2}/ρ_{w3} (13.7% compared with 21.6%). A small bias of 0.2% is computed for $(\rho_{w1} - \rho_{w3})/\rho_{w2}$, but the root-mean-squared difference is relatively large (22.0%). Thus errors in marine reflectance (see Table 5) partly compensate for the ratios and NDPI. The pigment concentration, however, should be measured independently for evaluation purposes.

Obviously the comparisons presented in Tables 5 and 6 and in Figs. 8 and 9 are not sufficient for drawing conclusions about the actual accuracy of the SIMBAD measurements of marine reflectance. More matchups acquired over a wide range of oceanic regimes need to be analyzed. Yet, even numerous matchups may provide only a relative answer. The error budget presented in Subsection 5.B should be considered as a good indicator of the actual accuracy.

7. Conclusion

A field radiometer, called SIMBAD, has been designed and built for the specific purpose of verifying satellite-derived ocean color. It measures aerosol optical thickness and diffuse marine reflectance in typical spectral bands of satellite ocean-color sensors. A preliminary study[16] had determined that measuring these variables concomitantly at the time of sat-

ellite overpass is necessary and generally sufficient for evaluating atmospheric correction algorithms. The radiometer is light, portable, and easy to operate. Any ordinary crew can quickly learn how to make measurements. Furthermore, the ship is not required to stop, making it possible to collect data during various research cruises and, in particular, on merchant ship voyages along regular routes in the world's oceans.

For diffuse marine reflectance, the radiometer is aimed at the ocean surface at a nadir angle of 45° and a relative azimuth angle of 135°. This viewing geometry allows one to reduce substantially, with the help of a polarizer, the skylight reflected by the surface in the instrument's field of view.[25] For aerosol optical thickness, the radiometer is aimed at the Sun like a classic sunphotometer. The same optics (field of view of 3°) and detectors, but different electronic gains, are used in both Sun- and sea-viewing modes. The radiometric measurements are made simultaneously in five spectral bands centered at 443, 490, 560, 670, and 870 nm, but sequentially in Sun- and sea-viewing modes. To transform water-leaving radiance into marine reflectance, we calculated the downward solar irradiance at the surface, which can be achieved accurately when the sky is clear or partly cloudy (i.e., the fractional coverage less than 0.2) and the Sun not obscured by clouds.

The inaccuracy of the SIMBAD aerosol optical thickness and diffuse marine reflectance, estimated theoretically, is adequate in view of the sensitivity of these variables to atmospheric correction. For marine reflectance, in particular, the theoretical accuracy is within the requirements for atmospheric correction errors, namely ± 0.002 in the blue and 3–4 times smaller in the green for clear waters.[10] The 5% inaccuracy objective specified by the SeaWiFS project,[61] however, will not be met for all waters. This is also the case with other instruments, even modern in-water instruments.[30] The SIMBAD radiometer has been evaluated at sea by comparing measurements by SIMBAD and other instruments (i.e., MER-2040 for diffuse marine reflectance and AATS-6 for aerosol optical thickness). There is agreement between the marine reflectance from SIMBAD and MER-2040 and between the optical thickness from SIMBAD and AATS-6, with comparison statistics generally consistent within expected levels of inaccuracy. Unlike MER, however, SIMBAD provides diffuse marine reflectance measurements almost directly.

The SIMBAD instrument measures in an angular geometry that may be different from that of satellite observation. When evaluating satellite retrievals against SIMBAD measurements, one should take into account the effects of angular differences, which are within $\pm 10\%$ for most remote-sensing conditions.[56] Making the proper corrections, however, is not simple. Bidirectional effects depend on the scattering phase function of the hydrosols, which is generally not known, and using average bidirectional factors[57] may introduce noise, as mentioned in Subsection 6.B. Furthermore, atmospheric correction schemes (e.g., those of Gordon[10] for SeaWiFS and MODIS) use an atmospheric transmittance that assumes a Lambertian water body.

Adequate sampling was achieved by building 10 SIMBAD radiometers for use in two complementary networks, one operated by the Laboratoire d'Optique Atmosphérique (LOA) at the University of Lille, France, the other by the Scripps Institution of Oceanography (SIO), California. The measurement program is based on ships of opportunity that participate on a volunteer basis or at a very little cost. The approach is complementary to dedicated evaluation experiments, which are expensive, cannot sample the wide range of expected atmospheric and oceanic conditions, and generally provide only a few matchups. Detailed information about the SIMBAD radiometer, including characteristics, measurement procedures and protocols, calibration history, and processing software, is available at http://www.loa.univ-lille1.fr/~simbad/ (LOA network) and at http://polaris.ucsd.edu/~simbad/ (SIO network), as well as in the data sets acquired since November 1996.

The SIMBAD radiometer has already proved useful for vicariously checking the radiometric sensitivity of the POLDER instrument onboard ADEOS and for evaluating POLDER ocean-color products.[19,62] The accuracy of the vicarious calibration coefficients was estimated to be better than 3%. A large decrease in the POLDER instrument response was detected in the blue spectral region, confirming the results previously obtained with alternative calibration techniques. The SIMBAD radiometer is currently being used in the same type of activities, but for SeaWiFS, MODIS, and MERIS, and will contribute, in a cost-effective way, to the evaluation of future ocean-color missions.

The SIMBAD radiometer was developed at the Laboratoire d'Optique Atmosphérique (LOA) of the Université des Sciences et Technologies de Lille, France, with funding from the Centre National d'Etudes Spatiales, the Centre National de la Recherche Scientifique, and the Région Nord–Pas-de-Calais. R. Frouin was supported by the National Aeronautics and Space Administration (NASA) and by the SIMBIOS Project. The authors wish to thank B. G. Mitchell and M. Kahru from the Scripps Institution of Oceanography (SIO) in La Jolla and P. B. Russell from the NASA Ames Research Center in Moffett Field for making available MER-2040 and AATS-6 data. The programming support of J.-M. Nicolas from LOA and of J. McPherson from SIO is gratefully acknowledged.

References

1. W. A. Hovis, D. K. Clark, F. Anderson, R. W. Austin, W. H. Wilson, E. T. Baker, D. Ball, H. R. Gordon, J. L. Mueller, S. Y. El Sayed, B. Sturm, R. C. Wrigley, and C. S. Yentsch, "Nimbus-7 Coastal Zone Color Scanner: system description and initial imagery," Science **210,** 60–63 (1980).
2. P.-Y. Deschamps, F.-M. Bréon, M. Leroy, A. Podaire, A. Bricaud, J.-C. Buriez, and G. Sèze, "The POLDER mission: in-

strument characteristics and scientific objectives," IEEE Trans. Geosci. Remote Sens. **32,** 3598–3615 (1994).
3. S. B. Hooker and W. Esaias, "An overview of the SeaWiFS project," EOS Trans. Am. Geophys. Union **74,** 245–246 (1993).
4. V. V. Salomonson, W. L. Barnes, P. W. Maymon, H. E. Montgomery, and H. Ostrow, "MODIS: advanced facility instrument for studies of the Earth as a system," IEEE Trans. Geosci. Remote Sens. **27,** 2145–2153 (1989).
5. M. Rast and J.-L. Bézy, "The ESA medium resolution imaging spectrometer (MERIS): requirements to its mission and performance of its system," in *Remote Sensing in Action, Proceedings of the 21st Annual Conference of the Remote Sensing Society*, P. J. Curran and C. Robertson, eds. (Remote Sensing Society, Nottingham, UK, 1985), pp. 125–132.
6. T. Nakajima, A. Higurashi, K. Aoki, T. Endoh, H. Fukushima, M. Toratani, Y. Mitomi, B. G. Mitchell, and R. Frouin, "Early phase emphasis of OCTS radiance data for aerosol remote sensing," IEEE Trans. Geosci. Remote Sens. **37,** 1575–1585 (1999).
7. J. E. Hansen and L. D. Travis, "Light scattering in planetary atmospheres," Space Sci. Rev. **16,** 527–610 (1974).
8. H. R. Gordon, J. W. Brown, and R. H. Evans, "Exact Rayleigh scattering calculations for use with the Nimbus-7 Coastal Zone Color Scanner," Appl. Opt. **27,** 862–871 (1988).
9. H. R. Gordon and M. Wang, "Retrieval of water-leaving radiance and aerosol optical thickness over the oceans with SeaWiFS: a preliminary algorithm," Appl. Opt. **33,** 443–452 (1994).
10. H. R. Gordon, "Atmospheric correction of ocean-color imagery in the Earth observing system era," J. Geophys. Res. **102,** 17,081–17,106 (1997).
11. R. W. Austin and T. J. Petzold, "The determination of the diffuse attenuation coefficient of sea water using the Coastal Zone Color Scanner," in *Oceanography from Space*, J. F. R. Gower, ed. (Plenum, New York, 1981), pp. 239–256.
12. A. Morel, "Optical modeling of the upper ocean in relation to its biogenous matter content (case 1 waters)," J. Geophys. Res. **93,** 10,749–10,768 (1988).
13. J. E. O'Reilly, S. Maritorena, B. G. Mitchell, D. A. Siegel, K. L. Carder, S. A. Garver, M. Kahru, and C. McClain, "Ocean color chlorophyll algorithms for SeaWiFS," J. Geophys. Res. **103,** 24,937–24,953 (1998).
14. J. L. Mueller and R. W. Austin, *Ocean Optics Protocols for SeaWiFS Validation, Revision 1*, NASA Tech. Memo. 104566, S. B. Hooker and E. R. Firestone, eds. (NASA Goddard Space Flight Center, Greenbelt, Md., 1995).
15. D. K. Clark, H. R. Gordon, K. J. Voss, Y. Ge, W. Broenkow, and C. Trees, "Validation of atmospheric correction over the oceans," J. Geophys. Res. **102,** 17,209–17,217 (1997).
16. M. Schwindling, P.-Y. Deschamps, and R. Frouin, "Validation of aerosol models for satellite ocean color remote sensing," J. Geophys. Res. **103,** 24,919–24,936 (1998).
17. M. Viollier, "Radiometric calibration of the Coastal Zone Color Scanner on Nimbus-7, a proposed adjustment," Appl. Opt. **21,** 6142–6145 (1982).
18. B. Fougnie, P.-Y. Deschamps, and R. Frouin, "Vicarious calibration of the POLDER ocean color spectral bands using *in-situ* measurements," IEEE Trans. Geosci. Remote Sens. **37,** 1567–1574 (1999).
19. R. E. Eplee, W. D. Robinson, S. W. Bailey, D. K. Clark, P. J. Werdell, M. Wang, R. A. Barnes, and C. R. McClain, "The calibration of SeaWiFS. II. Vicarious techniques," Appl. Opt. **40,** 6701–6718 (2001).
20. G. L. Clarke, G. C. Ewing, and C. J. Lorenzen, "Spectra of backscattered light from the sea obtained from aircraft as a measure of chlorophyll concentration," Science **167,** 1119–1121 (1970).
21. K. L. Carder and R. G. Steward, "A remote-sensing reflectance model of a red-tide dinoflagellate off west Florida," Limnol. Oceanogr. **30,** 286–298 (1985).
22. Z. P. Lee, K. L. Carder, R. G. Steward, T. G. Peacock, C. O. Davis, and J. L. Mueller, "Remote sensing reflectance and inherent optical properties of oceanic waters derived from above-water measurements," in *Ocean Optics XIII*, S. G. Ackleson and R. Frouin, eds., Proc. SPIE **2963,** 160–166 (1997).
23. Z. P. Lee, K. L. Carder, T. G. Peacock, and R. G. Steward, "Remote-sensing reflectance measured with and without a vertical polarizer," in *Ocean Optics XIII*, S. G. Ackleson and R. Frouin, eds., Proc. SPIE **2963,** 483–488 (1997).
24. C. D. Mobley, "Estimation of the remote-sensing reflectance from above-surface measurements," Appl. Opt. **38,** 7442–7455 (1999).
25. B. Fougnie, R. Frouin, P. Lecomte, and P.-Y. Deschamps, "Reduction of skylight reflection effects in the above-water measurements of diffuse marine reflectance," Appl. Opt. **38,** 3844–3856 (1999).
26. N. A. Krotkov and A. P. Vasilkov, "Reduction of skylight reflection effects in the above-water measurements of diffuse marine reflectance: comment," Appl. Opt. **39,** 1379–1381 (2000).
27. S. B. Hooker, G. Lazin, G. Zibordi, and S. McLean, "An evaluation of above- and in-water methods for determining water-leaving radiances," J. Atmos. Ocean. Technol. **19,** 486–515 (2002).
28. G. Zibordi, S. B. Hooker, J. F. Berthon, and D. D'Alimonte, "Autonomous above-water radiance measurements from an offshore platform: a field assessment experiment," J. Atmos. Ocean. Technol. **19,** 808–819 (2002).
29. S. B. Hooker and A. Morel, "Platform and environmental effects on above-water determinations of water-leaving radiances," J. Atmos. Ocean. Technol. **20,** 187–205 (2003).
30. D. A. Toole, D. A. Siegel, D. W. Menzies, M. J. Neumann, and R. C. Smith, "Remote-sensing reflectance determinations in the coastal ocean environment: impact of instrumental characteristics and environmental variability," Appl. Opt. **39,** 456–469 (2000).
31. H. Neckel and D. Labs, "The solar radiation between 3300 and 12500 Å," Sol. Phys. **90,** 205–258 (1984).
32. F. Kasten and A. T. Young, "Revised optical air mass tables and approximation formula," Appl. Opt. **28,** 4735–4738 (1989).
33. G. W. Paltridge and C. M. R. Platt, "Radiative processes in meteorology and climatology," in *Development in Atmospheric Science* (Elsevier, New York, 1977).
34. W. A. Hovis and J. S. Knoll, "Characteristics of an internally illuminated calibration sphere," Appl. Opt. **22,** 4004–4007 (1983).
35. G. Meister, P. Abel, R. Barnes, J. Cooper, C. Davis, G. Fargion, R. Frouin, M. Godin, D. Korwan, R. Maffione, C. McClain, S. McLean, D. Menzies, A. Poteau, J. Robertson, and J. Sherman, "Comparison of spectral radiance calibrations at oceanographic and atmospheric research laboratories," Metrologia **40,** S93–S96 (2003).
36. G. M. Keating, M. C. Pitts, and D. F. Young, "Improved reference models for middle atmosphere ozone (New CIRA)," in *Middle Atmosphere Program Handbook for MAP*, G. M. Keating, ed. (Scientific Committee on Solar-Terrestrial Physics Secretariat, U. of Illinois, Urbana, Ill., 1989), Vol. 31, pp. 37–49.
37. P.-Y. Deschamps, M. Herman, and D. Tanré, "Modeling of the atmospheric effects and its application to the remote sensing of ocean color," Appl. Opt. **22,** 3751–3758 (1983).
38. J.-L. Deuzé, M. Herman, and R. Santer, "Fourier series expansion of the transfer equation in the atmosphere–ocean system," J. Quant. Spectrosc. Radiat. Transfer **41,** 483–494 (1989).
39. D. Tanré, M. Herman, P.-Y. Deschamps, and A. de Leffe, "Atmospheric modeling for space measurements of ground reflec-

tances, including bidirectional properties," Appl. Opt. **18,** 3587–3597 (1979).
40. R. Frouin, D. Lingner, C. Gautier, K. S. Baker, and R. C. Smith, "A simple analytical formula to compute total and photosynthetically available solar irradiance at the ocean surface under clear skies," J. Geophys. Res. **94,** 9731–9742 (1989).
41. R. Frouin, M. Schwindling, and P.-Y. Deschamps, "Spectral reflectance of sea foam in the visible and near-infrared: *in-situ* measurements and remote sensing implications," J. Geophys. Res. **101,** 14,361–14,371 (1996).
42. B. Fougnie and P.-Y. Deschamps, "Observation et modélisation de la signature spectrale de l'écume de mer," in *Proceedings of the 7th International Colloquium on Physical Measurements and Signatures in Remote Sensing*, G. Guyot and T. Phulpin, eds. (Balkema, Rotterdam, 1997), Vol. 1, pp. 227–234.
43. J.-M. Nicolas, P.-Y. Deschamps, and R. Frouin, "Spectral reflectance of oceanic whitecaps in the visible and near infrared: aircraft measurements over open ocean," Geophys. Res. Lett. **28,** 4445–4448 (2001).
44. A. Ivanoff, "Polarization measurements in the sea," in *Optical Aspects of Oceanography*, N. G. Jerlov and E. S. Nielsen, eds. (Academic, New York, 1974), Chap. 8.
45. C. Cox and W. Munk, "Measurements of the roughness of the sea surface from photographs of the Sun's glitter," J. Opt. Soc. Am. **44,** 838–850 (1954).
46. A. Morel, "Optical properties of pure water and pure sea water," in *Optical Aspects of Oceanography*, N. G. Jerlov and E. S. Nielsen, eds. (Academic, New York, 1974), Chap. 1.
47. J. R. Zaneveld, D. M. Roach, and H. Pak, "The determination of the index of refraction of oceanic particulates," J. Geophys. Res. **79,** 4091–4095 (1974).
48. E. Aas, "The refractive index of phytoplankton," Inst. Rep. Ser. 46 (Institutt for Geofysikk, Oslo University, Oslo, Norway, 1981).
49. World Meteorological Organization (WMO), "A preliminary cloudless standard atmosphere for radiation computation," Reps. WCP-112 and WMO/TD 24 (World Meteorological Organization, Geneva, Switzerland, 1986).
50. B. Fougnie, R. Frouin, P.-Y. Deschamps, M. Chami, A. Poteau, and O. Hagolle, "Computations and measurements of polarized marine reflectance," in *Polarization Analysis, Measurements and Remote Sensing III*, D. B. Chenault, M. J. Duggin, W. E. Egan, and D. H. Goldstein, eds., Proc. SPIE **4133,** 191–201 (2000).
51. T. Matsumoto, P. Russell, C. Mina, W. Van Ark, and V. Banta, "Airborne tracking sunphotometer," J. Atmos. Ocean. Technol. **4,** 336–339 (1987).
52. J. M. Livingston, V. N. Kapustin, B. Schmid, P. B. Russell, P. K. Quinn, S. B. Timothy, A. D. Philip, and V. Freudenthaler, "Shipboard sunphotometer measurements of aerosol optical depth spectra and columnar water vapor during ACE 2," Tellus Ser. B **52,** 594–619 (2000).
53. T. Nakajima, A. Higurashi, K. Aoki, T. Endoh, H. Fukushima, M. Toratani, Y. Mitomi, B. G. Mitchell, and R. Frouin, "Early phase analysis of OCTS radiance data for aerosol remote sensing," IEEE Trans. Geosci. Remote Sens. **37,** 1575–1585 (1999).
54. K. J. Voss, E. J. Welton, P. K. Quinn, R. Frouin, M. Miller, and R. M. Reynolds, "2001: Aerosol depth measurements during the Aerosols99 experiment," J. Geophys. Res. **106,** 20,811–20,820 (2001).
55. B. G. Mitchell and M. Kahru, "Algorithms for SeaWiFS standard products developed with the CalCOFI bio-optical data set," in *CalCOFI Reports*, J. Olfe, ed. (Marine Life Research Group, Scripps Institution of Oceanography, La Jolla, Calif., 1998), Vol. 39, pp. 133–147.
56. H. R. Gordon and K. Ding, "Self-shading of in-water optical instruments," Limnol. Oceanogr. **37,** 491–500 (1992).
57. A. Morel and J. L. Mueller, "Normalized water-leaving radiance and remote sensing reflectance: Bidirectional reflectance and other factors," in *Ocean Optics Protocols for Satellite Ocean Color Sensor Validation, Revision 3*, NASA Tech. Memo. 2002-210004, J. L. Mueller and G. S. Fargion, eds. (NASA Goddard Space Flight Center, Greenbelt, Md., 2002), pp. 183–210.
58. O. Holm-Hansen, C. J. Lorenzen, R. W. Holmes, and J. D. H. Strickland, "Fluorometric determination of chlorophyll," J. Cons. Int. Explor. Mer. **30,** 3–15 (1965).
59. A. Morel and B. Gentili, "Diffuse reflectance of oceanic waters II: Bi-directional aspects," Appl. Opt. **32,** 6864–6879 (1993).
60. R. Frouin, P.-Y. Deschamps, B. G. Mitchell, and M. Kahru, "The Normalized Derived Phytoplankton Index for satellite ocean color applications," EOS Trans. Am. Geophys. Union **79,** 161 (1998).
61. C. R. McClain, W. E. Esaias, W. Barnes, B. Guenther, D. Endres, S. B. Hooker, B. G. Mitchell, and R. Barnes, *SeaWiFS Calibration and Validation Plan*, NASA Tech. Memo. 104566, S. B. Hooker and E. R. Firestone, eds. (NASA Goddard Space Flight Center, Greenbelt, Md., 1992).
62. B. Fougnie, M. Lecourt, J.-M. Nicolas, and P.-Y. Deschamps, "Validation of the POLDER ocean color algorithm using *in-situ* measurements and time series," in *ALPS 99 Symposium* (Centre National d'Etude Spatiales, Toulouse, France, 1999), Vol. 1, P04, pp. 1–4.